



University of HUDDERSFIELD

University of Huddersfield Repository

Fieldhouse, John D., Steel, William P. and Talbot, Chris J.

The measurement of the absolute displacement of a noisy disc brake

Original Citation

Fieldhouse, John D., Steel, William P. and Talbot, Chris J. (2008) The measurement of the absolute displacement of a noisy disc brake. *Proceedings of the Institution of Mechanical Engineers Part D Journal of Automobile Engineering*, 222 (7). pp. 1121-1140. ISSN 0954-4070

This version is available at <http://eprints.hud.ac.uk/id/eprint/2433/>

The University Repository is a digital collection of the research output of the University, available on Open Access. Copyright and Moral Rights for the items on this site are retained by the individual author and/or other copyright owners. Users may access full items free of charge; copies of full text items generally can be reproduced, displayed or performed and given to third parties in any format or medium for personal research or study, educational or not-for-profit purposes without prior permission or charge, provided:

- The authors, title and full bibliographic details is credited in any copy;
- A hyperlink and/or URL is included for the original metadata page; and
- The content is not changed in any way.

For more information, including our policy and submission procedure, please contact the Repository Team at: E.mailbox@hud.ac.uk.

<http://eprints.hud.ac.uk/>

The measurement of the absolute displacement of a noisy disc brake

J D Fieldhouse*, W P Steel, and C J Talbot

School of Computing and Engineering, University of Huddersfield, Huddersfield, UK

The manuscript was received on 18 March 2007 and was accepted after revision for publication on 7 April 2008.

DOI: 10.1243/09544070JAUTO582

Abstract: The investigation of in-plane vibration of a noisy disc brake is problematic because it is difficult both to measure and to verify. Because of the disc structure and the inability to visualize disc in-plane vibration, there has been reluctance by researchers to accept the contribution of a displacement parallel to the surface of the object, or in-plane displacement, to noise generation. In addition to measuring absolute displacement, it has been difficult to isolate the in-plane and out-of-plane components of displacement using either non-contact or conventional displacement measurement techniques. This paper investigates absolute displacement of a brake disc during noise generation. Double-pulsed holographic interferometry is used to record a series of time-related images of the brake head from three different angles of observation. Because each image views the brake head from a different perspective, each of them records a different degree of in-plane and out-of-plane displacement. By careful analysis of the three images, it is possible to isolate the in-plane displacement from the out-of-plane displacement. The time-related series allows the displacement to be investigated over a full cycle of excitation and so create an animation of the mode of vibration. It is seen that the in-plane displacement is complex and that its amplitude may be about twice that of the out-of-plane displacement.

Keywords: absolute displacement, noisy disc brake, in-plane vibration

1 INTRODUCTION

Developments in non-contact full-field measurement using double-pulsed holographic interferometry [1–5] have allowed accurate detection and measurement of out-of-plane disc mode measurement without the inherent problems associated with the use of accelerometers and discrete point measurements. Investigations by Talbot and Fieldhouse [6] developed the double-pulsed holographic technique to allow time-related interferograms to be recorded of both localized in-plane and full-field out-of-plane vibrations. The images were analysed to give data for the out-of-plane displacement field of the disc or other components on an unstable brake system, and then used to develop three-dimensional animation sequences that provide an

accessible image of the real vibrating system. Further work by Talbot and Fieldhouse [7] has shown how the data can also be analysed by mathematical techniques, such as Fourier series, to give information on the amplitude and phase of the displacement fields. Through the study of the holographic recordings of fringe patterns on the disc rim the work has shown that it is possible to analyse the in-plane components of displacement. The results have indicated that the in-plane displacement is of significantly large amplitudes, leading to the conclusion that future mathematical models should include the effects of in-plane displacement.

It is only relatively recently that scanning laser Doppler vibrometry (SLDV) and full-field electronic speckle pattern interferometry (ESPI) techniques have enabled the in-plane displacement characteristics to be determined for all brake components during noise generation.

The scanning laser Doppler vibrometer system PSV-400-3D, developed by Fischer and Bendel [8] at

*Corresponding author: School of Computing and Engineering, University of Huddersfield, Queensgate, Huddersfield, HD1 3DH, UK. email: j.d.fieldhouse@hud.ac.uk

Robert Bosch GmbH and in collaboration with Polytec GmbH, represents a commercially available tool that allows a brake system to be scanned during noise generation, with the measured displacement components individually or simultaneously represented as a dynamic animation sequence. Complementary work by Bendel *et al.* [9] has seen the system successfully applied to the measurement of in-plane and out-of-plane displacement of power tools. ESPI, developed by both Dantec Ettemeyer GmbH [10, 11] and Steinbichler Optotechnik GmbH [12], offers commercially available systems capable of time-related recordings and the full-field measurement of in-plane and out-of-plane vibration. Investigations undertaken by Krupta *et al.* [13] have successfully applied the 3D-PulseESPI system developed by Dantec Ettemeyer GmbH to the problem of a brake system generating noise. Unlike the SLDV, ESPI is a full-field technique making the measurement system much more conducive to brake noise studies. Work by Reeves *et al.* [14] used the ESPI technique to the measurement of out-of-plane displacements of a disc brake during noise generation. While the work demonstrates the ability of the ESPI technique to detect a moving mode of vibration about the disc, the comparative resolution of the images recorded is significantly lower than that typically recorded using holographic interferometry. The problem of resolution with the ESPI method is overcome in the systems developed by Dantec Ettemeyer GmbH [10, 11] and Steinbichler Optotechnik GmbH, where the images are analysed by post-processing software to produce an animated sequence of the disc displacement. Validations of the process and subsequent results have yet to be readily available and it is this aspect of such commercial packages that gives concern.

To complement the commercially available techniques of both SLDV and ESPI to in-plane measurement of a disc brake generating noise, the development of the holographic technique for the measurement of absolute vibrational displacement, both in plane and out of plane, has been continued by Fieldhouse and co-workers [15–17]. This work outlines a provisional methodology for the full-field recording of both in-plane and out-of-plane displacement of a twin-caliper brake system. Although the work is very much in its infancy, it has indicated that the in-plane magnitude is not insignificant and may be as much as three times that of the out-of-plane displacement. This paper outlines recent advances in the development of that technique.

2 EXPERIMENTAL DETAILS

The holographic theory behind absolute displacement measurement has been described in detail in earlier work [4, 15]. It was shown that, to measure and isolate the in-plane and out-of-plane displacements of any object, three holographic images are needed, all from a different viewing perspective, and that these have to be recorded simultaneously. The brake system used was of a system known to generate noise and one where extensive out-of-plane measurements had already been recorded. Using such a brake system guaranteed noise and served as a benchmark for the absolute displacement measurements and the extracted out-of-plane displacements. The following sections describe in detail the experimental equipment used and practical considerations made when developing the holographic system.

2.1 Optical arrangement

Figure 1 shows schematically the complete optical arrangement of the double-exposed holographic interferometry system used. The accompanying photograph helps the three-image optical arrangement to be understood. The system differs from the normal classical arrangement used for conventional displacement measurement, in which only the out-of-plane component of displacement was evaluated from a single holographic image, in that a further two plate holders and two associated reference beams are now required in order to evaluate the additional in-plane components of displacement.

The general distances of the illumination source S of the object beam and the observation positions O_1 , O_2 , and O_3 of the three plate holders, shown in Fig. 1 with respect to the centre of the disc, are given in Table 1. For reference the central points of each plate holder are used for the three observation points O_1 , O_2 , and O_3 and the centre of the -20 mm object lens for the source point S . The arrangement geometry is such that the centre O_1 , O_2 , or O_3 of each photographic plate holder is positioned to lie in a radial arc within the three-dimensional space around the brake head, the arc length for each holder being equal to the source point distance S from the brake head. The position of each observation direction O_1 , O_2 , and O_3 has been designed so as to minimize the sensitivity to one of the in-plane components d_x and d_y of displacement. The two plates O_1 and O_2 are aligned along the x axis at angles of 10° and 30° respectively and to the right of

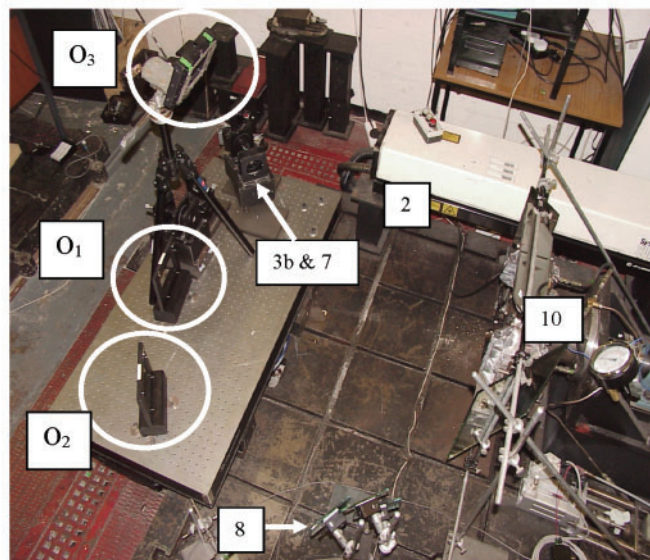
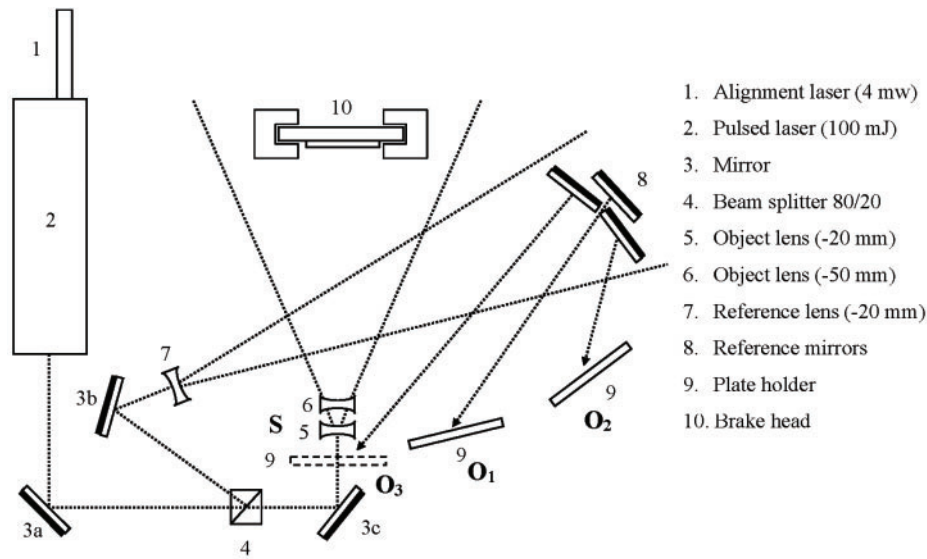


Fig. 1 Schematic diagram and photograph of the optical arrangement of the double-exposed holographic interferometry system used in the preliminary tests for measurement of in-plane and out-of-plane displacement components of a disc brake. Unlike conventional holographic interferometry, three holograms, O_1 [$10^\circ, 0^\circ$], O_2 [$30^\circ, 0^\circ$], and O_3 [$0^\circ, 30^\circ$], are recorded simultaneously by a reference beam subdivided by a special mirror arrangement (8) to provide three illumination directions

Table 1 Distance of the illumination and the three observation points from the centre of the disc

Observation direction	Distance (mm) with respect to the following		
	<i>x</i> axis	<i>y</i> axis	<i>z</i> axis
O_1	190	-70	1078
O_2	548	-70	948
O_3	0	549	948
Illumination direction S	0	0	1100

the origin, minimizing sensitivity to the d_y (vertical) component of displacement while maximizing d_x and d_z component sensitivities. The third plate at O_3

is aligned to the *y* axis and positioned 30° above the origin, minimizing the d_x (horizontal) component sensitivity while maximizing the sensitivities

to the d_y and d_z components. As a result, each holographic plate records a different absolute displacement.

Given that the geometries of the three observation points vary for each holographic plate, the developed interferometric images will each have a different perspective distortion. For analysis it is necessary to perform a spatial transform such that it is possible to 'map' points within the interferometric images to each other. Such a process is referred to as image processing.

3 IMAGE PROCESSING

The process of analysing the images is shown in Fig. 2. When each individual image has been processed, it is possible to combine the information in order to extract the absolute displacement and individual in-plane and out-of-plane displacements. Each process is described as follows.

3.1 Perspective correction

To facilitate perspective correction, four bolts are identified on the disc bell (Fig. 3(a)). Lines drawn

through these bolts form a reference rectangle, and their intercept with the disc rim, together with the rectangle diagonals, provide 12 control reference points (Fig. 3(b)). For each viewpoint the image of both the disc and the rectangle is deformed, thus returning the deformed quadrangle to its original shape will in turn eliminate the distortion observed in the disc.

The control point pairs in the target image and the reference images correspond to known points on the disc circumference and are used by an algorithm to calculate a spatial transformation function to map the coordinates (x, y) of all points in the target image to the coordinates (X, Y) of all points in the reference image. The function is based on the projective transformation function [18] given by

$$X = \frac{ax + by + c}{dx + ey + 1} \quad (1)$$

and

$$Y = \frac{fy + gy + h}{dy + ey + 1} \quad (2)$$

When an image is recorded, the four bolts may be

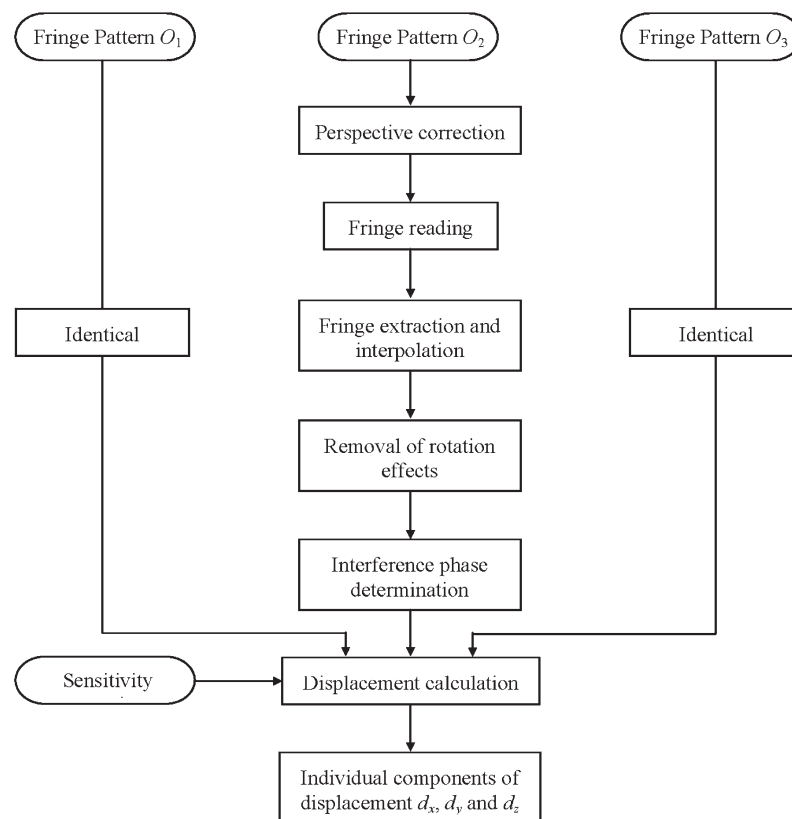


Fig. 2 Flow chart of image-processing steps to determine the components of displacement

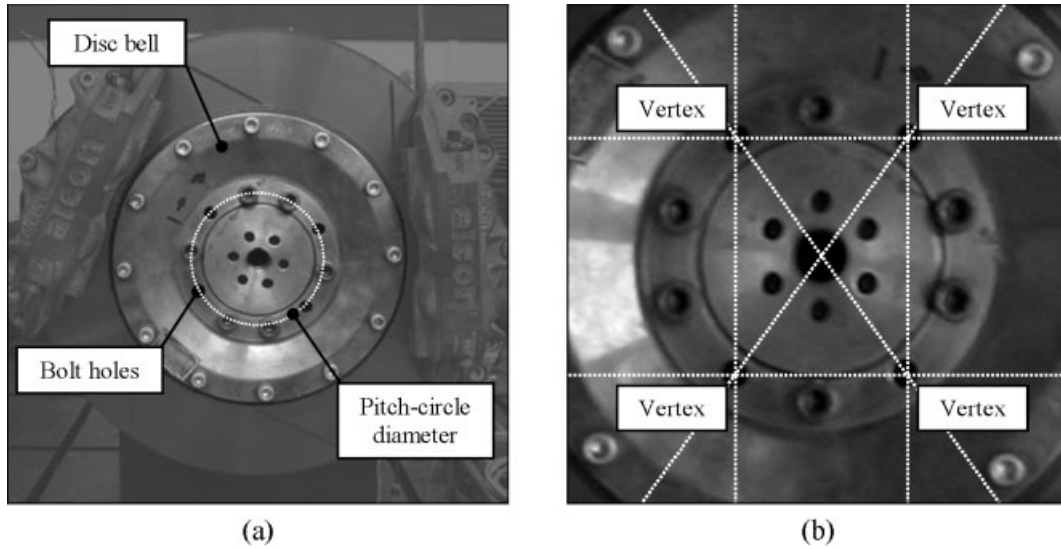


Fig. 3 Identification of reference image control points on the disc bell. (a) The bolt holes on the disc bell (highlighted) form the vertices of a rectangle. (b) Lines drawn between opposite vertex pairs can be used to calculate the centre of the disc and the coordinates of 12 known control points on the disc circumference

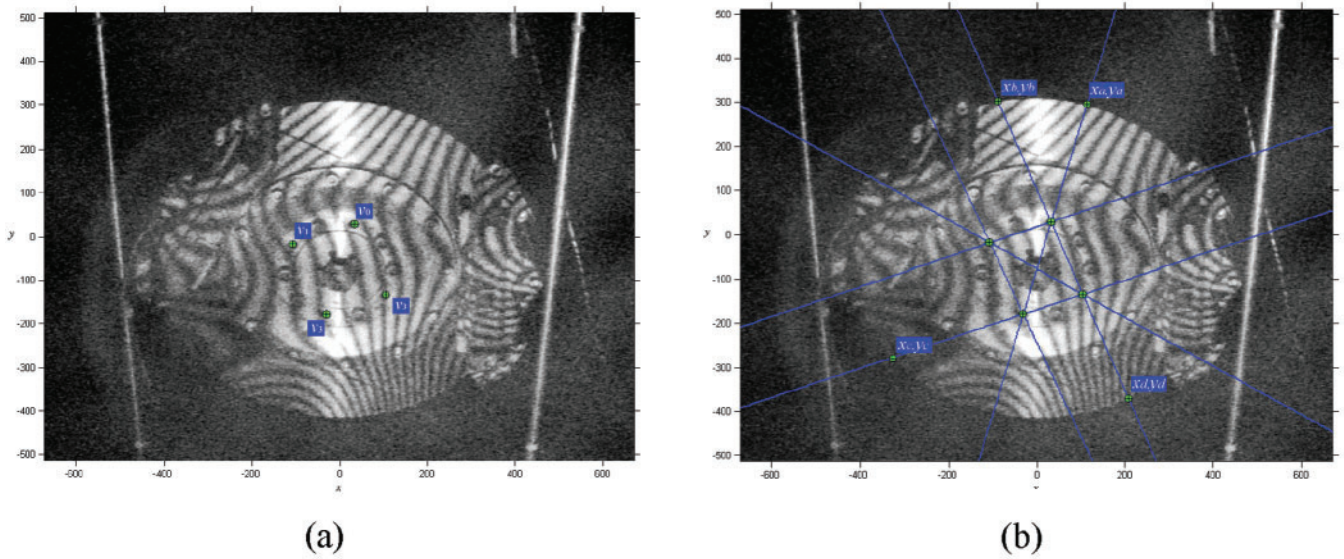


Fig. 4 Graphical selection of bolt hole vertices and control point in the target image. (a) The bolt holes on the disc bell from the vertices of a distorted rectangle $v_0, v_1, v_2,$ and v_3 , with the lines between opposite vertex pairs intersecting the circumference of the disc to form the control point coordinate $x_{a,b,c,d}$ and $y_{a,b,c,d}$

identified as shown in Fig. 4(a). From this the 12 reference points on the disc rim may be identified (Fig. 4(b)) and used to create a 400×400 reference grid, as shown in Fig. 5(a). The four corner points of the grid are used to create the ‘perspectively corrected’ image, as shown in Fig. 5(b). A circle of correct disc diameter is imposed on

the disc image to indicate the accuracy of the correction.

3.2 Fringe reading; fringe skeletonization using enhancement by spatial filtering

Fringe identification is relatively straightforward if manual processing is used. This can require a level of

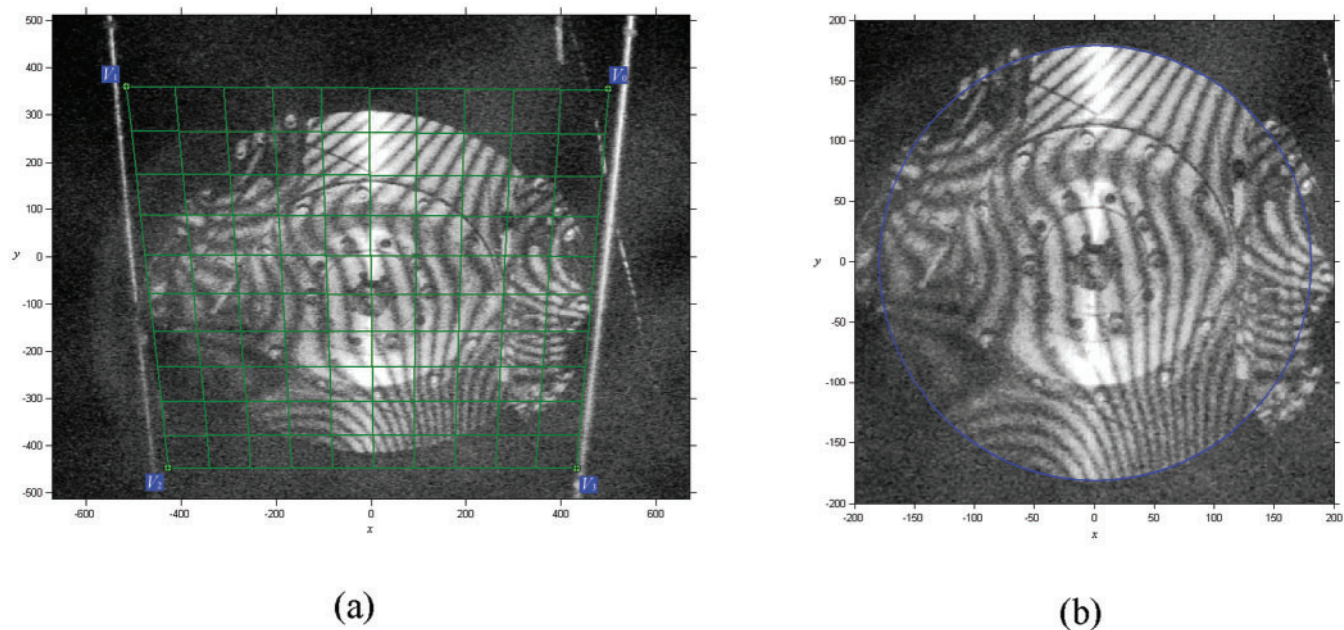


Fig. 5 (a) Image registration of the target image using a 400×400 grid of control points, derived from the initial set of control point coordinates $x_{a,b,c,d}$ and $y_{a,b,c,d}$ on the disc circumference. (b) The four corner vertices V_0 , V_1 , V_2 , and V_3 of the grid form the set of control points used to return the perspective corrected reference image

skill and, when broad fringes are recorded, a degree of error may be introduced when trying to identify the centre of the fringe. Consider the grey-scale image in Fig. 6(a); it can be seen that the spread of the intensity profile of pixels along the horizontal

scan line covers a significant number of the 256 grey-scale intensity levels. The points of regional minimum intensity values along the profile represent the position of the dark fringes, and the regional maxima represent the bright fringes. As a

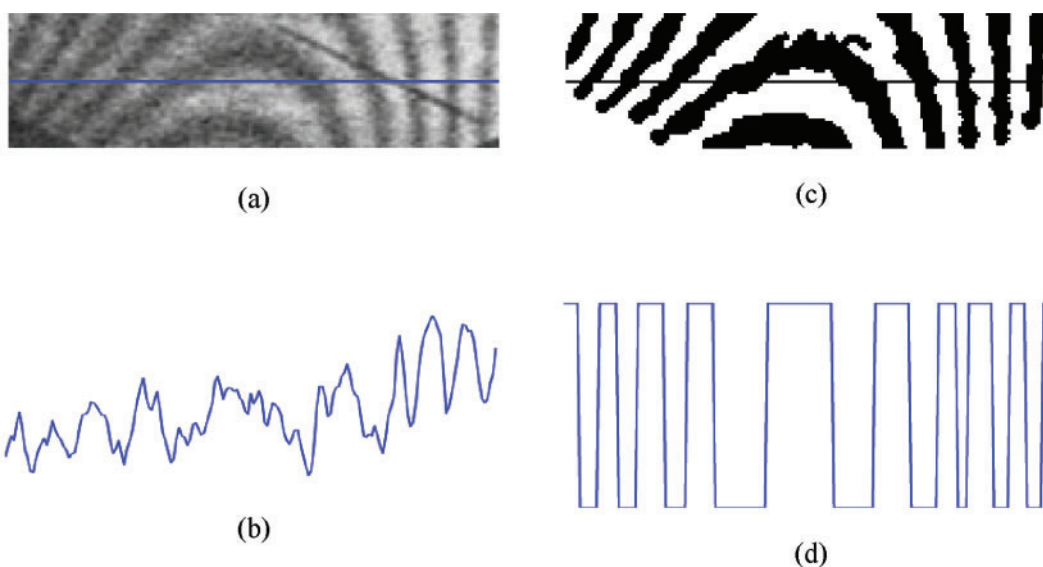


Fig. 6 Effects of image enhancement on fringe skeletonization. The uneven intensity distribution in the grey-scale image in (a) results in a large variation in regional maximum and minimum intensity trace as shown in (b). In the spatial filtered image the regional maximum and minimum in (c) vary between either 1 or 0, making the dark fringes more readily identifiable as shown in the intensity trace in (d)

consequence of the uneven intensity distribution in the grey-scale image the regional maximum and minimum values vary significantly along the scan line. For example the first bright fringe and the last dark fringe along the scan line have approximately the same intensity level. This makes it difficult to set a threshold grey level for the identification of the dark fringes needed for skeletonization. Practically it would be necessary to identify all regional maximum and minimum values corresponding to the bright and dark fringes and to adjust the spread of the intensity levels along the profile such that all regional maxima had values close to 255 (white) and all regional minima had values close to 0 (black). It would then be possible to find the position of all pixels below a minimum level along the scan line, which would correspond to a point on the fringe line. Such a process would not identify the centre point of each fringe but only the darkest point on the fringe; this would increase the possibility that points that lie on the same fringe would not be coincident between adjacent scan lines, resulting in a broken skeletonized fringe line.

In the intensity profile for the enhanced binary image shown in Fig. 6(b), the intensity levels of pixels along the scan line varies between either 0 (black) and 1 (white). The problems associated with small fluctuations in the intensity profile, resulting in unwanted regions of maximum and minimum intensity levels, owing to speckle and uneven intensity distribution in the grey-scale image, have been removed by spatial filtering. The regional minimum or zero regions corresponding to the dark fringes are more readily identifiable than in the equivalent grey-scale intensity profile, and determine not only the location of the fringe but also its width. In this way the centre of each fringe line is identified and extracted, as opposed to the darkest point on the fringe being identified from the grey-scale intensity profile (Fig. 6(a)). By extracting the centre-line of each fringe the probability of breaks in the skeletonized fringe line are significantly reduced.

The spatial filtered image is obtained by filtering out unwanted data in the image such as speckle. The fringe pattern in the resulting image will be enhanced and unwanted background objects removed [19]. The process is to apply a low-pass filter and a very-low-pass filter. The function of the low-pass filter is to calculate the mean grey level value in the neighbourhood in which a spatial mask is located. The mean grey level is then calculated by dividing the sum by the number of pixels in the mask, e.g. $1/9$ for a 3×3 mask. In this way, low-pass

filtering can be used to remove high-frequency spatial components in the image such as speckles, while leaving low frequencies untouched. This results in a general blurring of the image in a process that is often referred to as neighbourhood averaging (Fig. 7(a)). If a very-low-pass filter is applied to the image, such that the size of the $n \times n$ spatial mask is increased, the averaging area will be larger, and the effect will be to blur out the uneven intensity distribution in the image, enhancing the very-low-spatial-frequency components. If the very-low-pass filtered image is subtracted from the low-pass filter image, the fringe pattern in the resulting image will be enhanced and unwanted background objects removed. Such an image is shown in Fig. 7(c). Removal of unwanted background objects leaves a clear fringe pattern suitable for automatic fringe identification (Fig. 7(d)).

Figure 8 shows the results of scanning the skeletonized images in the x direction (Fig. 8(a)) and the y direction (Fig. 8(b)). It is clear that care needs to be taken to ensure that full information on the fringe pattern is maintained, and so both images are added to give the overall pattern (Fig. 8(c)). In some instances the fringe lines are not complete; therefore linking together interrupted fringe lines is necessary and accomplished with a procedure referred to as 'bridging'. In essence this identifies missing pixels and completes the fringe pattern. This process is followed by identification of fringe order (numbering) and identification of direction. This process still requires manual assistance.

Having identified the fringe order and direction the absolute two-dimensional surface plot may be calculated as shown in Fig. 9. This includes rotation, which must be removed to give the absolute disc in-plane and out-of-plane displacements.

3.3 Derotation

Rotation of the disc is seen as straight fringe lines as shown typically in Fig. 10 for the three observation positions. The pattern is that of a disc 'tilting' and, as such, may be readily subtracted from the two-dimensional images of the disc surface plot, as shown in Fig. 9. The same process of calculating the two-dimensional image may be used for the disc rotation, such plots being shown in Fig. 11. If this information (Fig. 11) is subtracted from the raw data (Fig. 9) (or the full disc information, as shown in Fig. 12), the absolute displacement of the disc may be determined as a two-dimensional plot as shown in Fig. 13. It will be noted when comparing Fig. 12(b)

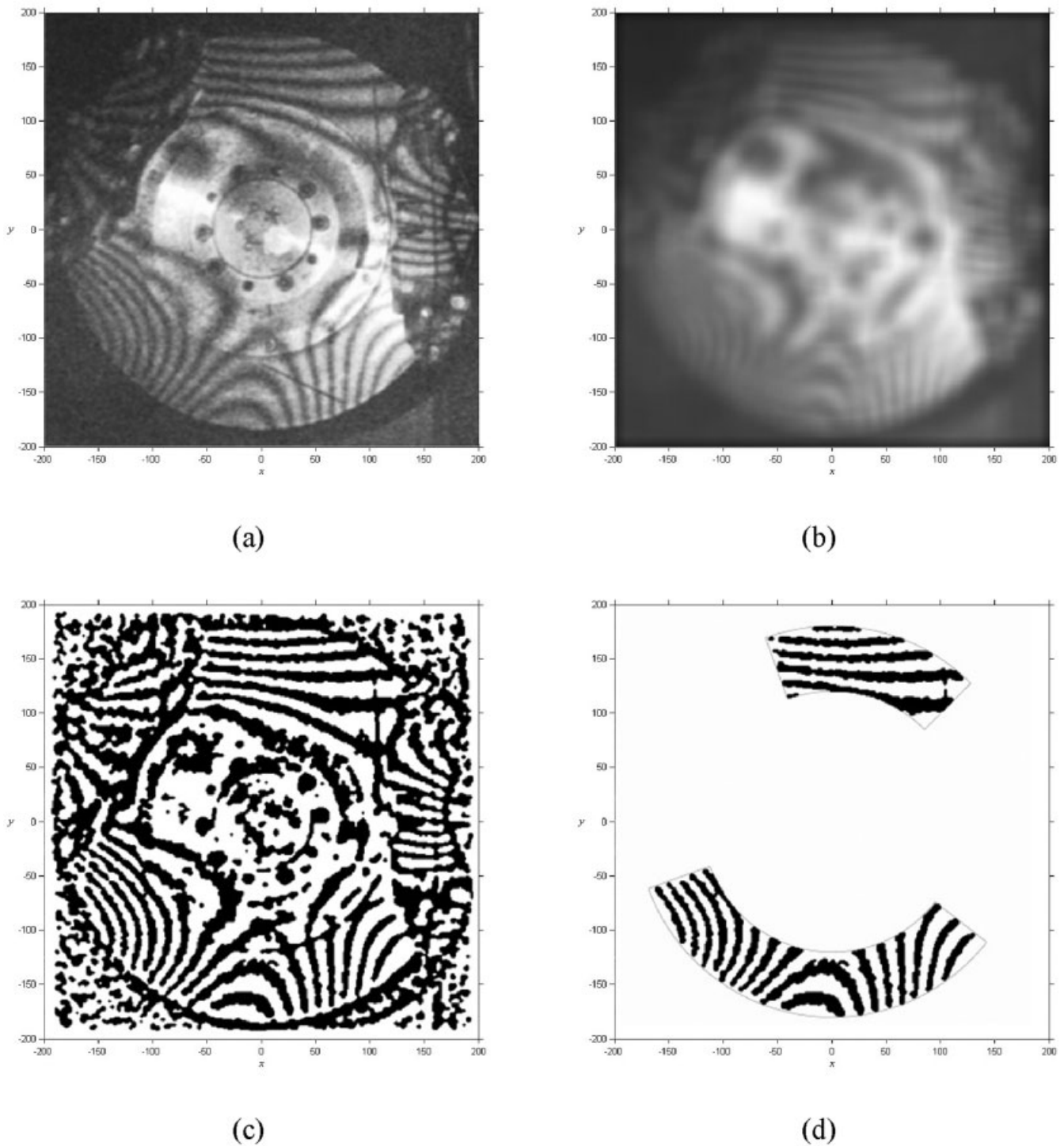


Fig. 7 Fringe pattern enhancement by spatial filtering: (a) low-pass filtered image with a 3×3 spatial mask; (b) very-low-pass filtered image with a 20×20 spatial mask; (c) image resulting from subtraction of (a) from (b) and binary conversion; (d) removal of unwanted background objects

and Fig. 13(b) that with the non-derotated image an antinode is suppressed in the lower section of the disc. This demonstrates the importance of correct

image processing; the entire mode order may be misrepresented if the raw data are not correctly processed.

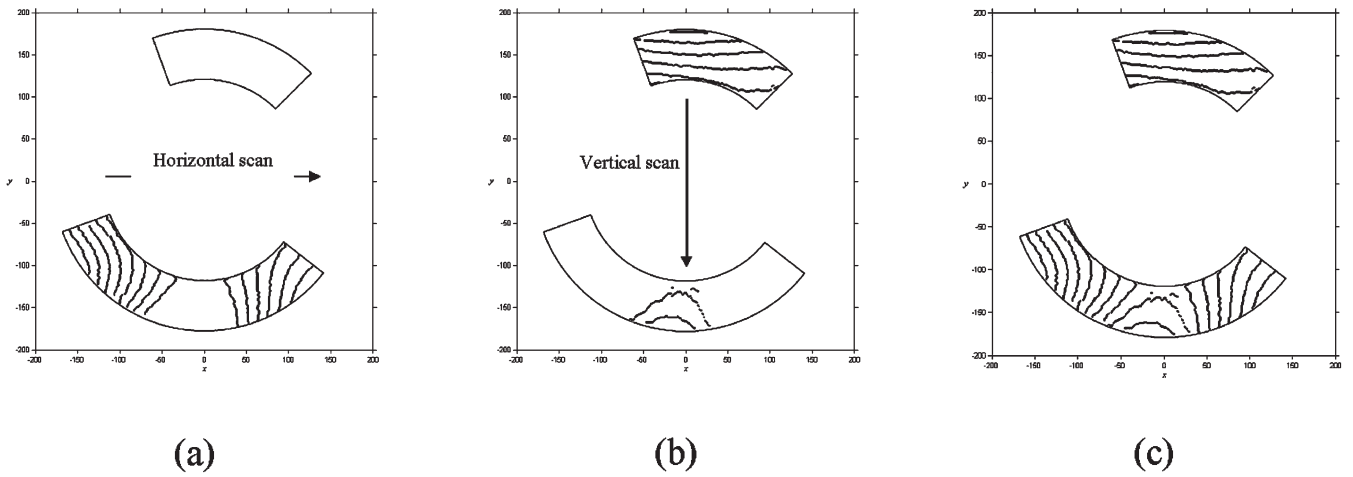


Fig. 8 Skeletonization of the enhanced binary image using a scanning algorithm. The two separate skeletonized images shown are for the (a) horizontal and (b) vertical scan directions. It can be seen that the scanning direction affects the accuracy and reliability of the skeletonized fringe line. One is added to the other to produced the combined image in (c)

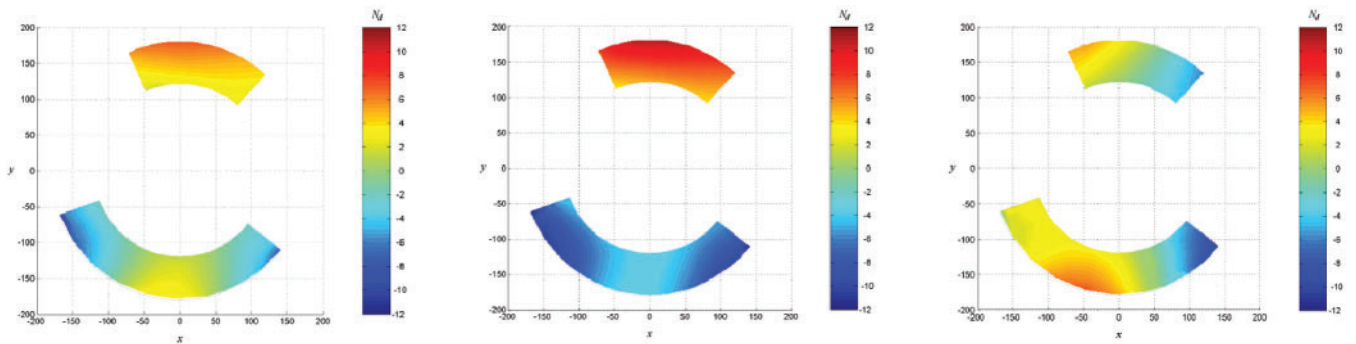


Fig. 9 Set of two-dimensional coloured surface plots of the interpolated fringe order arrays N_d , for the different observation directions O_1 , O_2 , and O_3

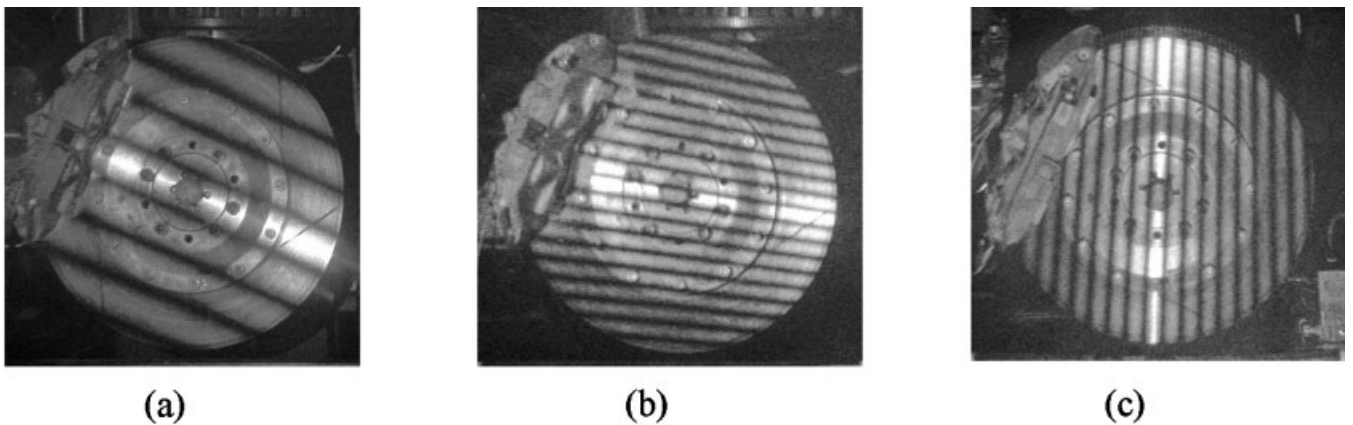


Fig. 10 Perspective-corrected images of pure rotation of disc rotating at 8.5 r/min (single-caliper arrangement shown): (a) 10° horizontal; (b) 30° horizontal; (c) 30° vertical

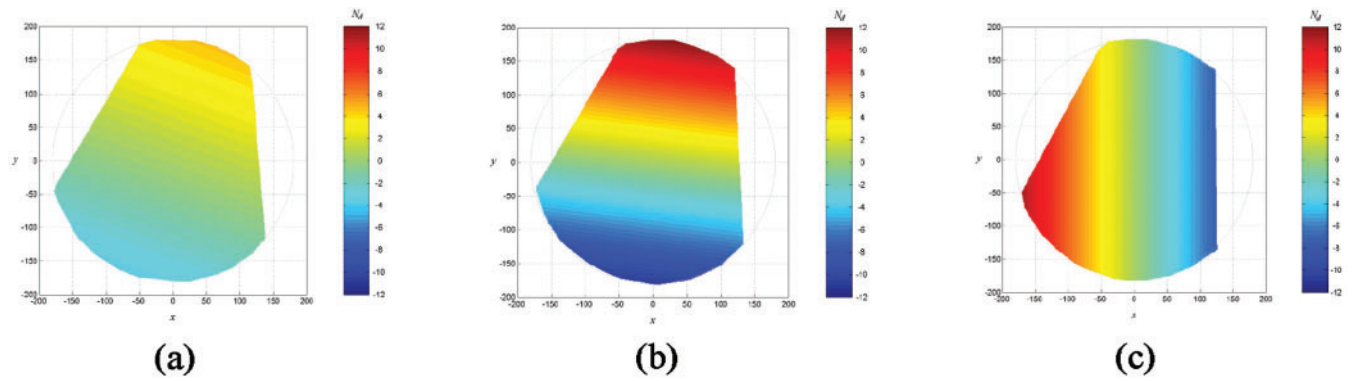


Fig. 11 Set of two-dimensional coloured surface plots of the calculated interference order arrays due to a 10 r/min clockwise rotation of the disc for the three different observation directions

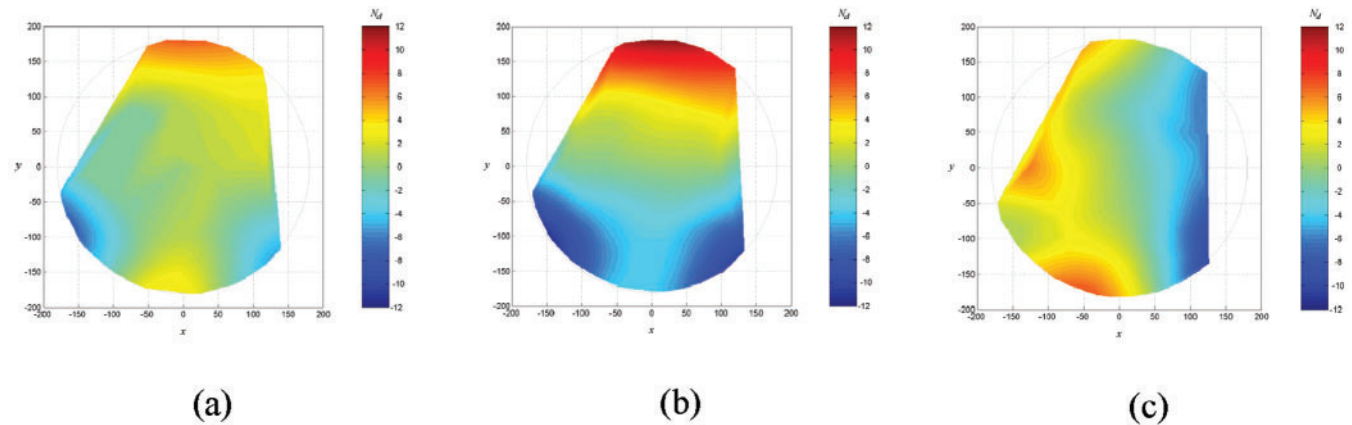


Fig. 12 Set of two-dimensional coloured surface plots of the interpolated fringe order arrays, for the different observation directions O_1 , O_2 , and O_3

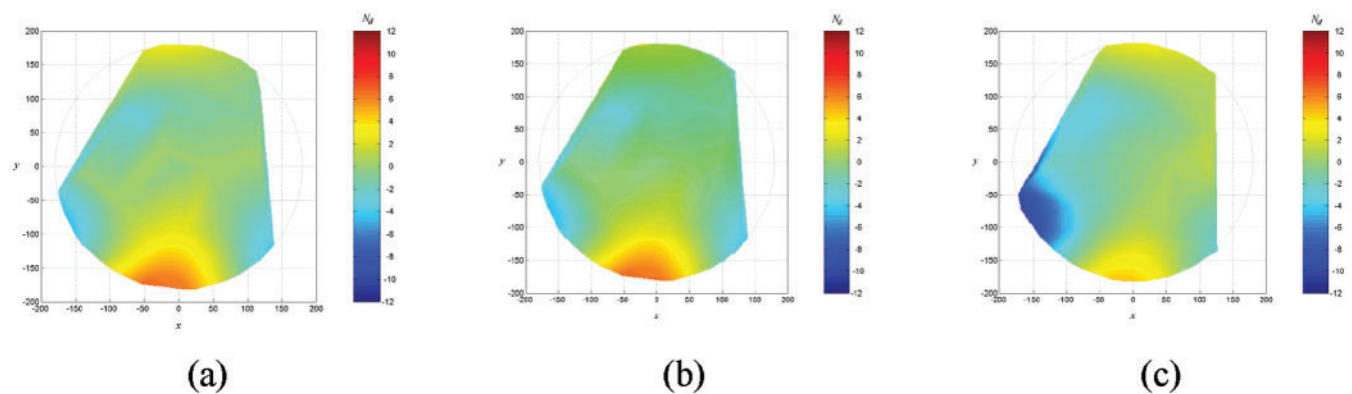


Fig. 13 Set of two-dimensional coloured surface plots of the interference order arrays due to disc vibration, for the three different observation directions. The effects of the 10 r/min clockwise rotation of the disc having been 'subtracted' from the interpolated fringe order is shown in Fig. 12

3.4 Processing of the interference patterns

The processing of the interference pattern is extensive as it involves around 11 holograms for each observation viewpoint per half-cycle, some 33 'raw' holograms. Each requires perspective correction, derotation, and then fringe analysis. The method of fringe reading remains a purely empirical process and constitutes a significant amount of the processing time required in determining the displacement components from the interferometric images. The methodology adopted for numbering the fringes uses the results from the interference pattern models to build upon the fringe-reading techniques as outlined in earlier work [15]. In some respects the advantage of a series of time-related images over a single set of images is that the development of the fringe patterns can be seen from one image to the next. This proves particularly useful when assigning the fringe order number (in effect the amplitude from the zero position) and direction to each fringe in the image.

The final stage in retrieving the individual components of the displacement vector involves the processing of the three phase arrays, as described in the foundation work [17], for each set of interferometric images in the time series, and follows the same process. The resulting series of combined displacement components determined from the 11 sets of interferometric images of the disc brake are shown in the expanded work [20]. Typical results are presented in Fig. 14. The x - y , or in-plane, displacement is represented by a series of arrows and is shown separately in Fig. 15, referred to as a 'quiver' plot. The length and direction of the arrows are related to the magnitude and direction respectively of the displacement. The out-of-plane component of displacement in the z axis is shown separately in Fig. 16 as a three-dimensional coloured surface plot. In each set of images a wire frame represents the zero position of the disc and also defines the boundary of the evaluated points for the upper and lower halves of the disc.

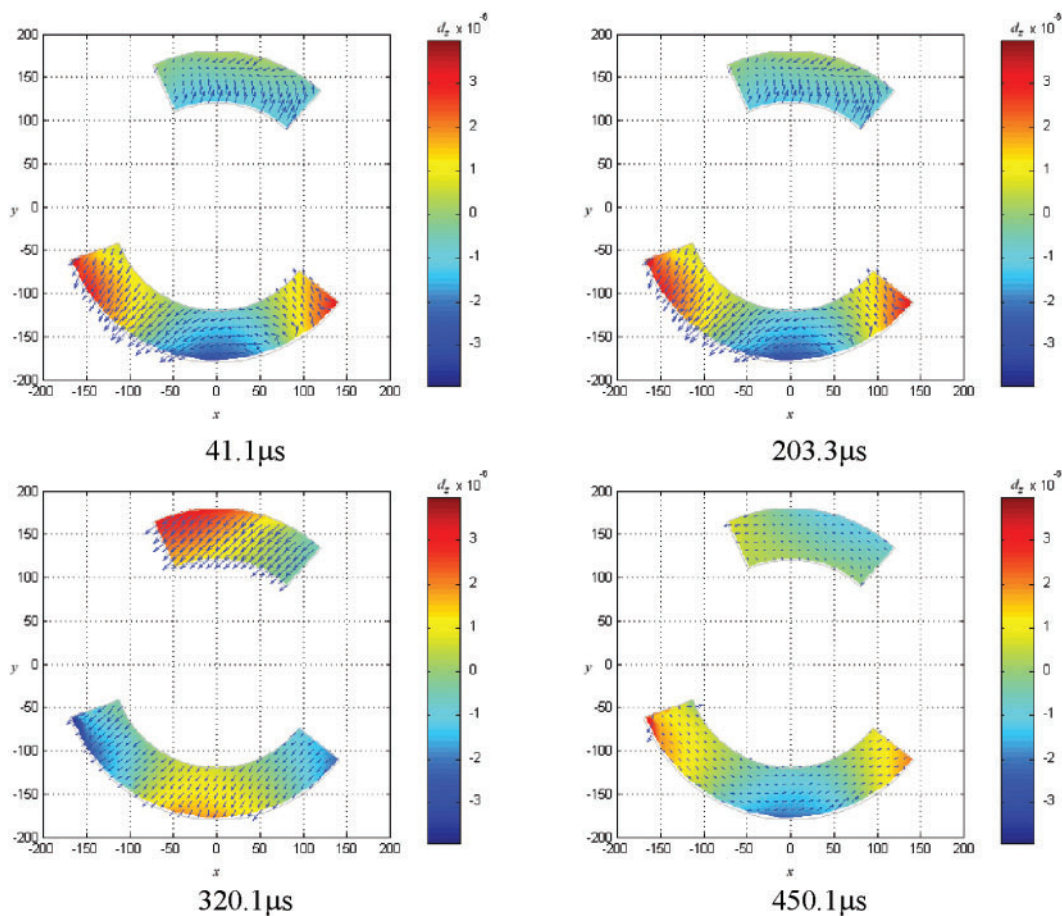


Fig. 14 Combined two-dimensional quiver and coloured surface plots for the simultaneous representation of the in-plane and out-of-plane displacement, vector components d_x , d_y , and d_z , for the recorded time series

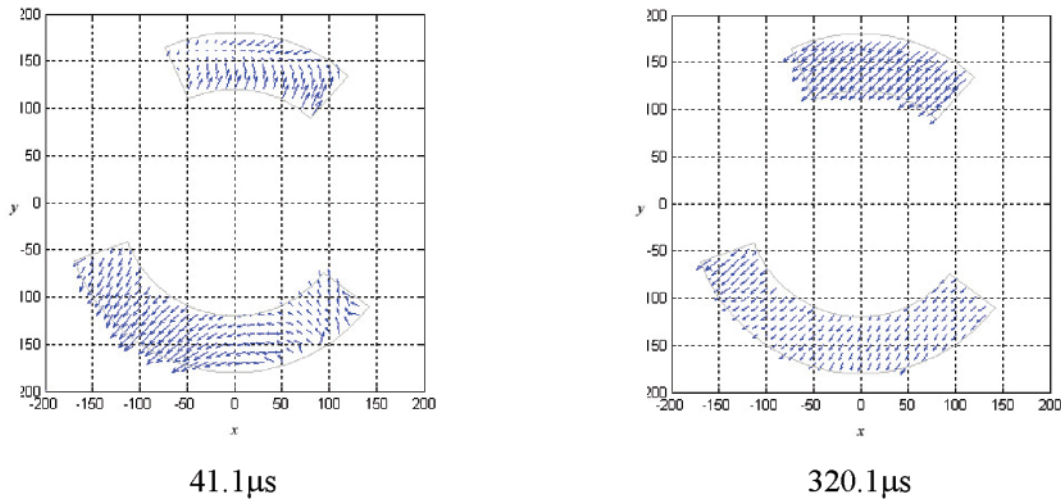


Fig. 15 Two-dimensional quiver plot of the in-plane displacement, vector components d_x and d_y , for the recorded time series

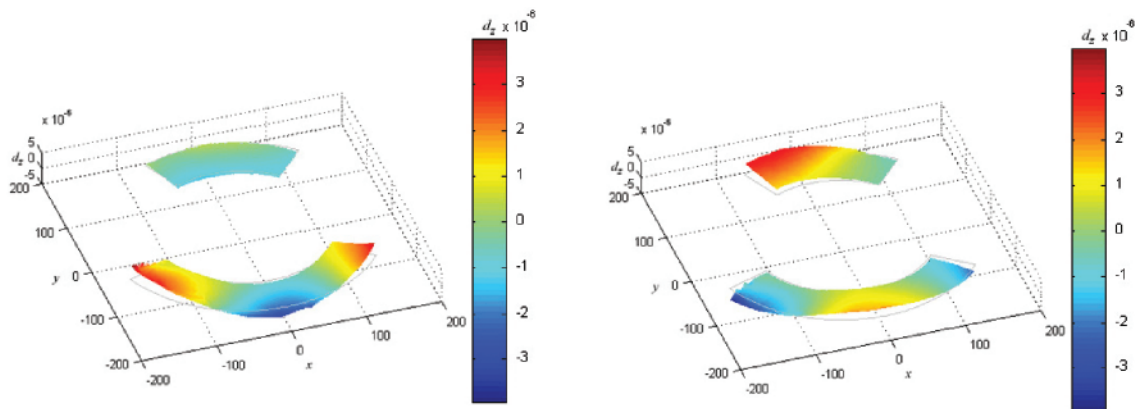


Fig. 16 Three-dimensional coloured surface plot of the out-of-plane displacement, vector component d_z , for the recorded time series

3.5 Extension of in-plane vibration, from quiver plot to in-plane surface plot

The in-plane displacement is generally represented as a two-dimensional quiver plot of the type shown in Fig. 15. In the plot the arrows are representative of vectors calculated from the displacement vector components d_x and d_y relative to a surface point in the x - y plane. The use of a quiver plot is generally satisfactory for observing the in-plane displacement for a single position in the vibration cycle; however, because the vector is calculated relative to the same fixed point in the x - y plane, the method can lead to misinterpretation when observing the in-plane disc mode behaviour over a time-related series. Consider Figs 17(a) and (b), which show the quiver plot representations of two vectors calculated from the displacement vector components d_x and d_y for sequential time base positions t_1 and t_2 in the vibration cycle. As both vectors are calculated

relative to the same initial surface point in the x - y plane, this implies that the in-plane displacement is moving away from this point. The true representation of the displacement vector between time base positions t_1 and t_2 is shown in Fig. 17(c). It is clear that the two vectors are not moving in the same direction, with the vector at t_2 moving in the opposite direction back towards the fixed surface point.

In order to visualize the in-plane mode of displacement better, an algorithm was developed to represent the d_x and d_y displacement vector components as a two-dimensional surface plot. In this way the surface movement of the disc due to the in-plane mode could be more readily observed over the time series. Such a process is shown in Fig. 18 where the quiver plot in Fig. 18(a) is better represented as a surface plot in Fig. 18(c).

Such a two-dimensional plot may be attributed to the real disc surface which tends to enhance the

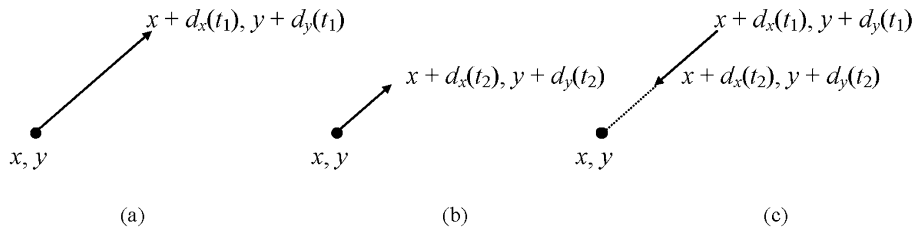


Fig. 17 Quiver representation of displacement vector components d_x and d_y relative to a fixed surface point for successive time base positions (a) t_1 and (b) t_2 , which imply that the vectors are moving in the same direction. (c) The true representation of the vector at t_2 is that it is moving in the opposite direction to t_1 , back toward the surface point

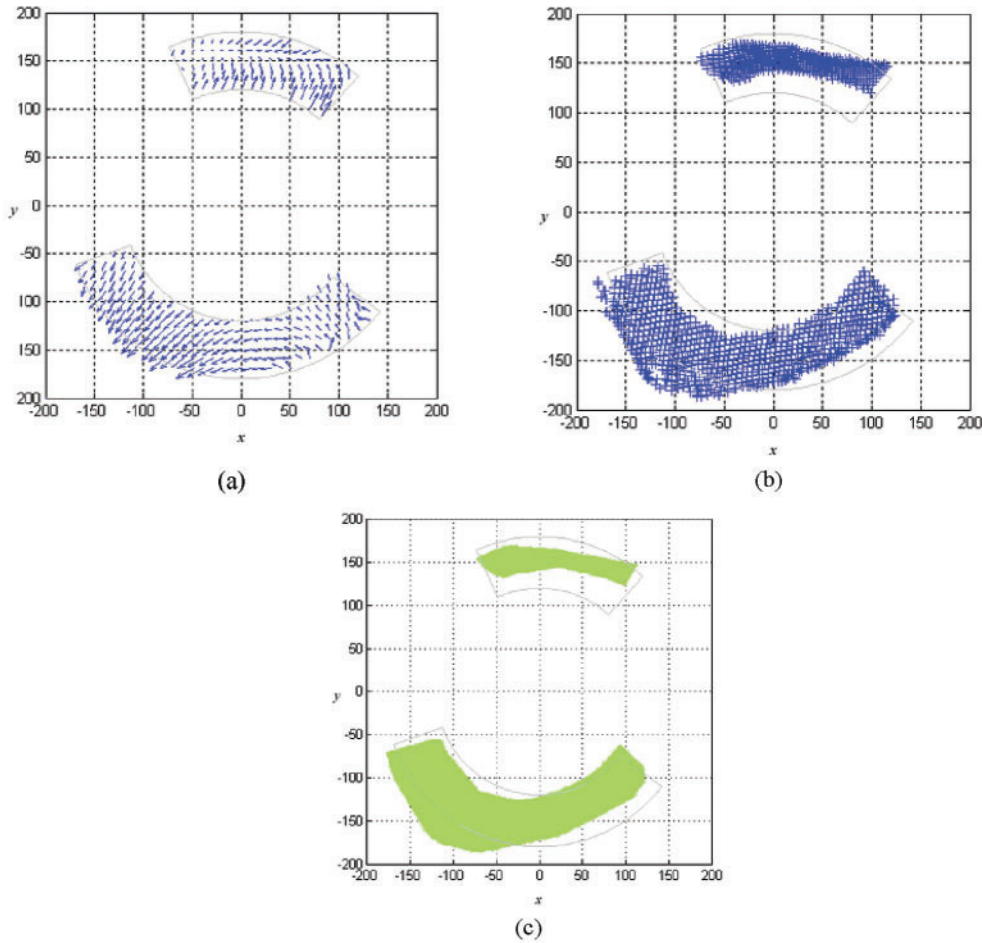


Fig. 18 Representation of the in-plane displacement, vector components d_x and d_y , for the interpolated $45.4 \mu s$ time base position using (a) a two-dimensional quiver plot and (b) the equivalent scaled two-dimensional plot of extracted data points. (c) The interpolated data points for the upper and lower halves of the disc are used to produce a continuous two-dimensional surface plot

overall understanding of the combined in-plane and out-of-plane modes of vibration, as shown in Fig. 19.

4 DISPLACEMENT ANALYSIS OF DISCRETE SURFACE POINTS

As discussed earlier there is a significant advantage in using the technique of holographic interferometry

for displacement measurement in that it facilitates full-field measurement of the surface of an object simultaneously. Given the resulting interferometric images of the disc, and through calculation of the displacement vector components for all points on its surface, it is then possible to examine the individual displacement vector components at any discrete point on the surface of the disc. In this way the

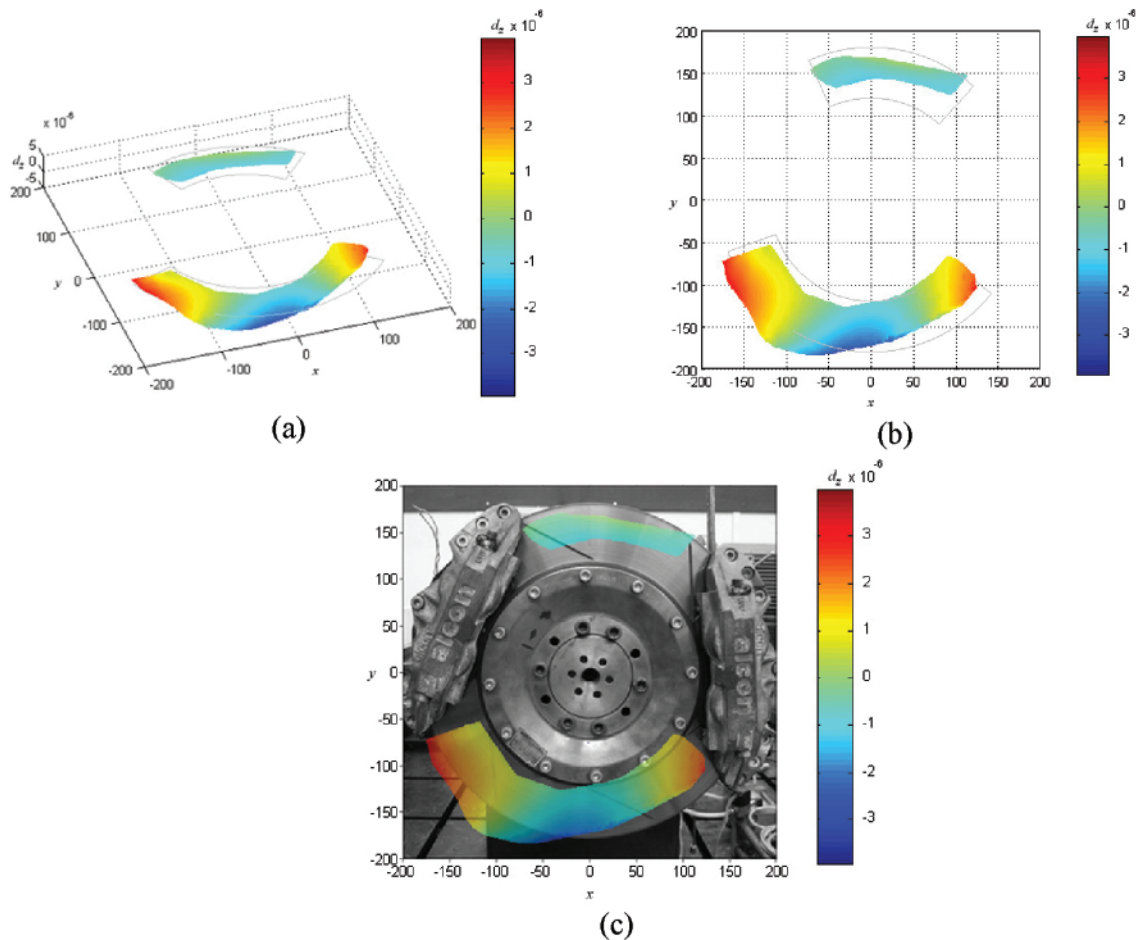


Fig. 19 Simultaneous representation of the in-plane and out-of-plane displacement, vector components d_x , d_y , and d_z , for the interpolated $45.4 \mu\text{s}$ time base position. The data can be presented either as (a) a three-dimensional or (b) a two-dimensional coloured surface plot with associated colour scale. (c) Alternatively a semitransparent two-dimensional surface plot can be superimposed on an image of the disc

frequency and phase relationships of the vector components may be examined in detail. Consider Fig. 20, which shows the general front view of the brake head together with 20 labelled points positioned at 10° increments on a 150 mm radius around the surface of the disc. For each point P1, P2, ..., P20, the individual displacement vectors d_x , d_y , and d_z have been interpolated for each time base position within the out-of-plane vibration cycle.

In general, it can be seen that, for the in-plane displacement components in the upper disc section (Figs 21(a) to (d) – a selection from the eight measurement points), the displacement of the disc possibly indicates a degree of periodic movement with the maximum and minimum in-plane displacements occurring at approximately $50 \mu\text{s}$ and $310 \mu\text{s}$ respectively, in all the graphs. Because there is no clear reference position for the out-of-plane displacement, these in-plane values are difficult to

relate to the out-of-plane displacement with regard to establishing a meaningful phase relationship. For example in Figs 21(a) and (b) the transition out-of-plane displacements occur at about $100 \mu\text{s}$ and $300 \mu\text{s}$ whereas in Figs 21(c) and (d) they are at about $200 \mu\text{s}$ and $440 \mu\text{s}$. This would imply that there may be a moving out-of-plane mode of vibration which was seen with this section of the disc changing between holding either one or two anti-nodes [15]. Because of this behaviour, attributing a meaningful phase relationship to the in-plane mode is difficult. This observation may be further supported by the apparent 180° phase difference between the in-plane components and the out-of-plane component occurring at approximately $310 \mu\text{s}$, shown in Figs 21(c) and (d), where the displacement components are seen to be at their apparent minimum and maximum values respectively. This is not seen in the other images.

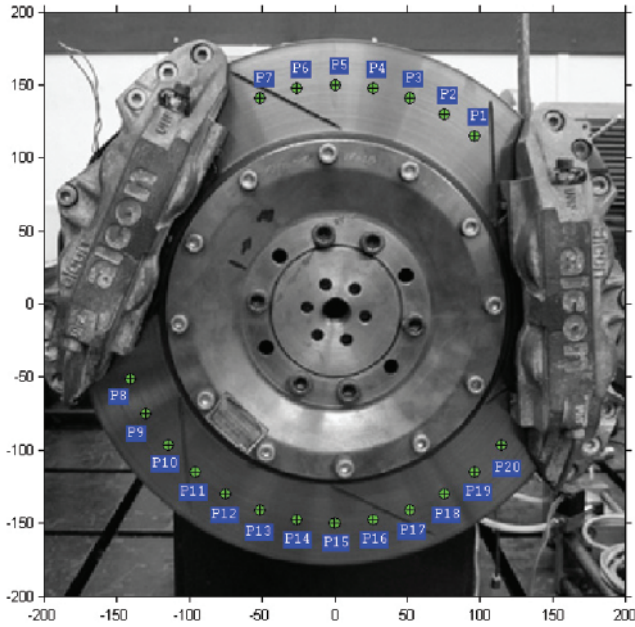
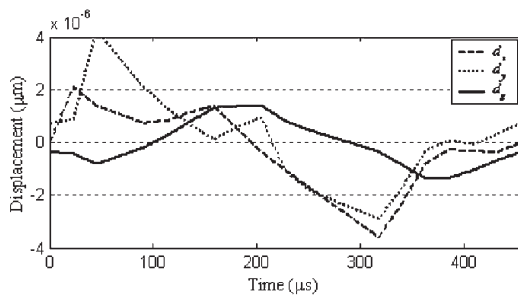
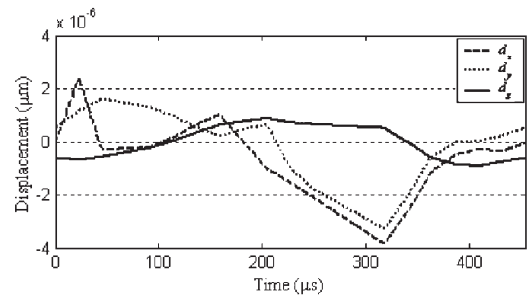


Fig. 20 General front view of the brake head together with 20 discrete measurement points positioned at 10° increments on a 150 mm radius around the surface of the disc

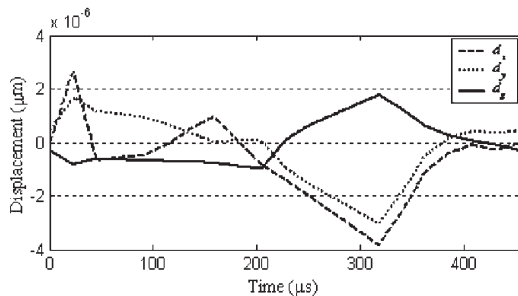
The displacement vector component plots for the upper disc section would tend to indicate that, over the out-of-plane vibration period of 454 μs (2203 Hz), the in-plane displacement of the disc tends to exhibit a greater magnitude of downward displacement (top to bottom) than upward displacement (bottom to top). This is particularly evident at around 310 μs where, as discussed, the disc appears to reach its apparent limit of downward movement in both x and y at approximately 4 μm, which is double the equivalent maximum upward movement. This difference may be the result of the difference between the sizes of the upper and lower disc sections, with any upward movement in the smaller upper disc section being constrained by the closer positioning of the left-hand and right-hand pad pairs, resulting in an overall tendency for the disc to move more easily in the downward direction. The two in-plane displacement components d_x and d_y appear to have generally equal magnitudes and directions (positive or negative) over the out-of-plane vibration period, suggesting that any movement of the disc would be diagonal at an angle of



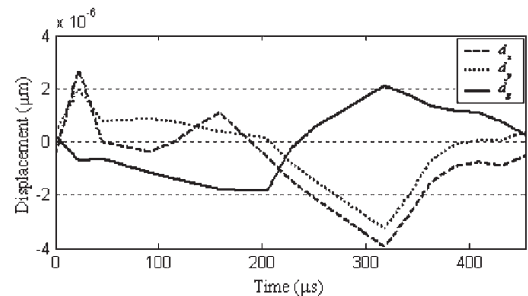
(a) Point 1 - 50°



(b) Point 3 - 70°



(c) Point 5 - 90°



(d) Point 7 - 110°

Fig. 21 Plots of displacement vector components d_x , d_y , and d_z in the upper section of the disc as a function of time for each point P1, P2, ..., P8 identified in Fig. 20

approximately 45° . This is supported by additional results (not presented).

The in-plane displacement components in the lower disc section (Figs 22(a) to (f) – a selection from the 12 measurement points) tend to mirror approximately the profile of the equivalent displacement components in the upper disc section and similarly indicate a degree of periodic movement. With the lower section of disc the out-of-plane mode appears to be more stable as seen by the transition position at about $150\ \mu\text{s}$ and $385\ \mu\text{s}$. This gives an estimated out-of-plane frequency of $2127\ \text{Hz}$ ($2203\ \text{Hz}$ as recorded). The in-plane mode is significantly more complex, exhibiting a frequency at about twice that of the out-of-plane frequency. In this case the two minimum values of in-plane displacement occur at approximately $50\ \mu\text{s}$ and $280\ \mu\text{s}$ ($4348\ \text{Hz}$). Because both modes are relatively stable and periodic, it is a little easier to establish an approximate phase relationship. The graphs shown in Figs 22(c), (d),

and (e) show the transition points at about the same time of $350\ \mu\text{s}$, which would suggest that they are in phase at these positions on the disc.

With the larger lower section of the disc the relative magnitudes of each of the three calculated displacement components can be examined by considering the maximum, minimum, and mean values of all discrete surface points in the interpolated time series for both the upper and the lower disc sections (Table 2). Included in the analysis is the resultant of the d_x and d_y in-plane displacement components, which is identified as d_{xy} .

Analysis of the magnitudes of the two modes indicate that for the upper disc section the in-plane mode d_{xy} is 2.15 times the magnitude of the maximum out-of-plane mode, at $6.704\ \mu\text{m}$ and $3.106\ \mu\text{m}$ respectively. A similar comparison for the two modes in the lower disc section indicates that the ratio of the in-plane displacement to the out-of-plane displacement is 2.25 for values of $8.932\ \mu\text{m}$ and

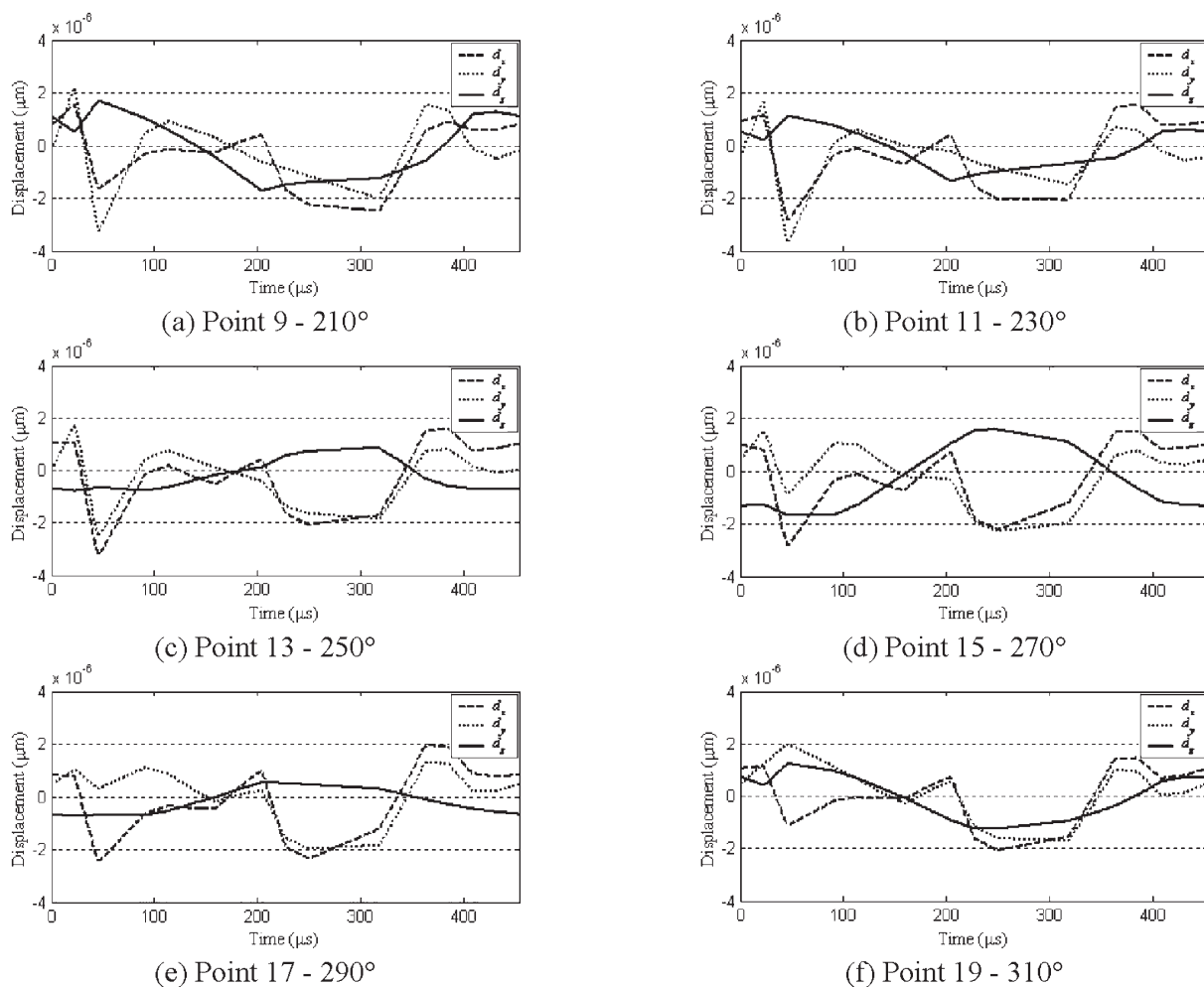


Fig. 22 Plots of displacement vector components d_x , d_y , and d_z , in the lower section of the disc as a function of time for each point P9, P10, ..., P20 identified in Fig. 20

Table 2 Maximum, minimum, and mean values of displacement in the upper and lower disc sections

Displacement component	Displacement value (μm)		
	Maximum	Minimum	Mean
<i>Upper disc section</i>			
d_x	3.527	-4.845	-0.727
d_y	5.701	-4.139	-0.202
d_{xy} (in plane)	6.704	-	1.743
d_z (out of plane)	3.106	-2.375	-0.022
<i>Lower disc section</i>			
d_x	4.515	-7.306	-0.306
d_y	4.437	-6.409	-0.202
d_{xy} (in plane)	8.932	-	1.536
d_z (out of plane)	3.964	-3.934	-0.136

3.964 μm respectively. It is significant to note that the ratios of the two modes are consistent for both sections of the disc irrespective of the fact that the magnitudes of both the in-plane and the out-of-plane displacements are higher in the lower disc section. The discrepancies between the observed amplitudes of the two disc sections would indicate that the movement of the disc in the smaller upper disc section is constrained by the pad pair, while the larger lower disc section is less constrained, allowing greater movement of the disc.

5 VALIDATION OF RESULTS

Figure 23 compares a holographic recording from earlier work carried out in 2000 [21] with an image,

10° to the horizontal, recorded during this work. The earlier work was of a 2000 Hz frequency recording and was not concerned with time-related holograms; therefore no time during the cycle is available. However, the two images possess a fair degree of similarity regarding antinode positions. Within the variables of pressure, temperature, time, disc speed, and angular viewing differences, it is felt that there is support for the fact that the recording process is validated. Validation by comparison with earlier results may be seen in work by Talbot and Fieldhouse [7] where the fringes on the rim of the disc confirm the presence of in-plane vibration.

The 'moving' mode indicated in the upper section may be seen in earlier work [15] as shown in Fig. 24. Figure 24(a) shows two antinodes in the upper

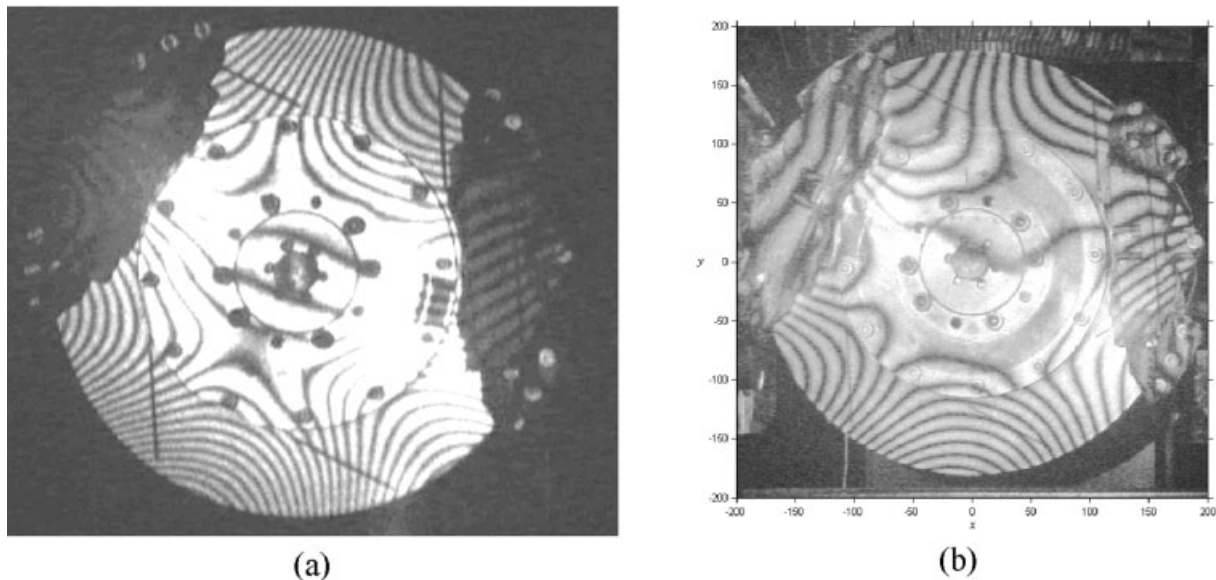


Fig. 23 Comparisons of the same brake system recorded in 2002 during noise investigations. The optical arrangement was such as to measure only out-of-plane displacement, as in the image in (a). The image in (b) was of the same brake as viewed from observation point 2, i.e. 10° to the horizontal

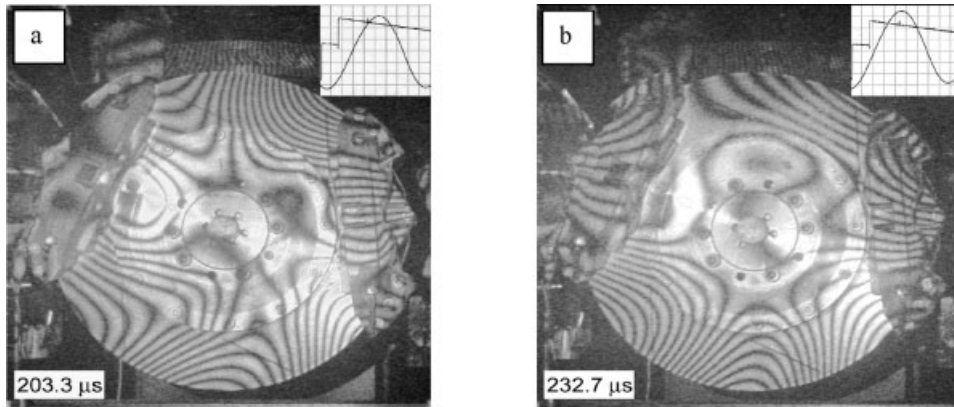


Fig. 24 Images of the twin-caliper system at different points within the cycle [15]. Note the relative stable position of the antinodes in the lower disc section whereas the upper section exhibits two antinodes in the image in (a) and one antinode in (b). Note also the displacement of the right-hand caliper (fringe pattern), which is very similar. The left-hand caliper changes as the antinodes in the upper section change

section whereas Fig. 24(b) shows one antinode. As the number of antinodes changes in the upper section, the mode of the left-hand caliper is seen to change, implying that it 'accepts' the moving antinode between the pad-disc interface.

Observations of in-plane vibrations have been analysed by observing the behaviour of the fringes as seen on the rim of a disc during vibration and rotation [15]. The analysis considers both opposed pistons and sliding fist types of caliper. It is pertinent to note that there is a difference between the amplitudes and phases of both sides of the disc blade. With the opposed piston the sides are generally in phase and of equal amplitude. With a sliding fist type the caliper is less rigid and this is seen in the edge fringe pattern. The 'neutral' axis of face in-plane displacement is not acting along the centre of the disc blade and is offset towards the outboard side. This means that the displacement on the inboard side is greater than the outboard face which is an indication of a greater frictional force at the inboard face as opposed to the outboard face. The opposed piston type is substantially more rigid and, as such, the 'neutral' axis is closer to the centre-line of the disc blade. Not only is this seen in the fringe pattern, but also it is often observed in thermal images. There is more variation in temperature across the disc width with a sliding fist type than with an opposed piston type.

6 CONCLUSION

The work has demonstrated that it is possible, using double-pulsed holographic interferometry, to find the

full-field amplitudes and phases of both the out-of-plane displacement and the in-plane displacement of a disc brake generating noise. This represents the first significant application of holographic interferometry for the measurement of in-plane displacement in automotive disc brakes.

The methods employed for recording the time-related series and for the recovery of the individual displacement vector components have been validated both by a series of experimental checks and thorough consideration of the history of previous research from which the current holographic system has been developed.

The development of a two-stage registration algorithm, for the removal of perspective distortion in the image using points on the disc surface, has been shown to represent an improvement in the mapping accuracy and reliability of the holographic images over the method established in earlier investigations [14–16]. In automating the extraction of the fringe lines by implementing a group of fringe detection algorithms, a method is developed which reduces the necessity for manual input and offers a 20 per cent reduction in processing time, over the fringe evaluation methods used in previous work, together with offering general improvements in both reliability and accuracy.

The developed method of interpolation has enabled the individual or simultaneous representation of the in-plane and out-of-plane displacement as a three-dimensional animation sequence. This is a particularly useful means to demonstrate the results to people not in the field and/or with non-scientific backgrounds. A significant advantage offered with the interpolation methods outlined is that the

displacement analysis can be carried out for a set of displacement components at any point on the disc surface and for any time base position within the cycle of excitation of the disc. This now facilitates detailed analysis of both the magnitude and the phase relationship of the individual in-plane and out-of-plane displacement characteristics of the disc brake system to be determined for the recorded vibration period. In this respect the work does not provide a solution to a noisy brake system but it will add significantly to the understanding of the complex mechanisms involved.

The work is more extensive than before, with validation being carried out through reference to earlier work and repeat results to confirm repeatability.

The relationship between the in-plane and out-of-plane modes is complex. In the upper smaller section of disc the out-of-plane mode is not stable. It exhibits a 'moving' mode in that it cycles between accommodating one and then two antinodes, so making a phase relationship difficult to determine. The lower section exhibits more stability with a measured out-of-plane frequency of 2127 Hz compared with 2203 Hz noise frequency. This would indicate that the analytical process loses very little information during manipulation of the images. More significantly the in-plane mode of vibration appears to be twice that of the out-of-plane frequency at an estimated 4348 Hz. It is not clear why this should be the case and it may be a special phenomenon seen only with the two-caliper arrangement.

It is also seen that the in-plane mode is more complex than simply radial or circumferential; it is a combination of the two. The combination would suggest equal contributions in the x and y directions with the movements being in phase, as shown in both sections of the disc.

The work also is now capable of producing two-dimensional plots of the in-plane displacement, which significantly improves interpretation and understanding by both the researcher and the designer.

The unstable mode of a twin-caliper arrangement is extremely complex. Because of this the work will continue with a simpler single-caliper system in order to understand better the more conventional arrangement.

REFERENCES

- 1 **Felske, A.** and **Hoppe, G.** Vibration analysis by double pulse laser holography. SAE paper 7700330, 1980.
- 2 **Felske, A., Hoppe, G.,** and **Matthäi, H.** Oscillations in squealing disc brakes – an analysis of vibration modes by holographic interferometry. SAE paper 780333, 1980.
- 3 **Murakami, H., Tsunda, N.,** and **Kitamura, T.** A study concerned with a mechanism of disc brake squeal. SAE paper 841233, 1984.
- 4 **Nishiwaki, M., Haranda, H., Okamura, H.,** and **Ikeuchi, T.** Study on brake squeal. SAE paper 890864, 1989.
- 5 **Fieldhouse, J. D.** and **Newcomb, P.** Double pulsed holography used to investigate noisy brakes. *Optics Lasers Engng*, 1996, **25**, 455–494.
- 6 **Talbot, C.** and **Fieldhouse, J. D.** Investigation of in-plane disc vibration using laser holography. SAE paper 2002-01-2607.
- 7 **Talbot, C.** and **Fieldhouse, J. D.** Fourier analysis of holographic data from a noisy disc brake and its implication for modelling. *Proc. Instn Mech. Engrs, Part D: J. Automobile Engineering*, 2003, **217**(11), 975–984.
- 8 **Fischer, M.** and **Bendel, K.** Hot on the trail of squealing brakes. Application report, LM INFO: laser measurement systems, issue 1, 2004, pp. 8–9.
- 9 **Bendel, K., Fischer, M.,** and **Schüssler, M.** Vibrational analysis of power tools using a novel three-dimensional scanning vibrometer. In Proceedings of the Sixth International Conference on *Vibration measurements by laser techniques: advances and Applications*, in Proceedings of the SPIE, Ancona, Italy, vol. 5503, 22–25 June 2004, pp. 177–184 (SPIE, Bellingham, Washington).
- 10 **Wang, Z.** and **Ettemeyer, A.** Pulsed ESPI to solve dynamic problem. Application report 04-97, Dr Ettemeyer GmbH & Co., Neu-Ulm, Germany, 1997.
- 11 **Wang, Z., Walz, T.,** and **Ettemeyer, A.** 3D-pulse ESPI technique for measurement of dynamic structure response. In Proceedings of the 18th Modal Analysis Conference: Conference and Exhibition on *Structural dynamics (IMAC XVIII)*, in Proceedings of SPIE, San Antonio, Texas, USA, vol. 4062(2), 2000, pp. 1362–1368 (SPIE, Bellingham, Washington).
- 12 **Mayer, T., Schubert, B.,** and **Steinbichler, H.** Pulsed laser ESPI technology as a quantitative modal testing technique. In Proceedings of the 25th International Conference on *Noise and vibration engineering (ISMA 25)*, Leuven, Belgium, 2000 (Katholieke Univeriteit Leuven, Leuven).
- 13 **Krupka, R., Walz, T.,** and **Ettemeyer, A.** New techniques and applications for 3D-brake vibration analysis. In Proceedings of the 18th Annual Brake Colloquium and Engineering Display, San Diego, California, USA, 1–4 October 2000, SAE paper 2000-01-2772 (SAE International, Warrendale, Pennsylvania).
- 14 **Reeves, M., Taylor, N., Edwards, C., Williams, D.,** and **Buckberry, C. H.** A study of brake disc modal behaviour during squeal generation using high-speed electronic speckle pattern interferometry and near-field pressure measurement. *Proc. Instn*

- Mech. Engrs, Part D: J. Automobile Engineering*, 2000, **214**(3), 285–296.
- 15 Fieldhouse, J. D., Talbot, C., Steel, W. P., and Crampton, A.** The measurement of in-plane vibration characteristics of a noisy twin caliper disc brake. In *Internoise 2003, Proceedings of the 32nd International Congress and Exposition on Noise Control Engineering*, Jeju, Republic of Korea, 25–28 August 2003, pp. 135–142.
- 16 Talbot, C., Fieldhouse, J. D., Steel, W. P., and Crampton, A.** Modelling in-plane and out-of-plane vibrations in disc brake squeal. In *Internoise 2003, Proceedings of the 32nd International Congress and Exposition on Noise Control Engineering*, Jeju, Republic of Korea, 25–28 August 2003, pp. 3003–3011.
- 17 Steel, W. P., Fieldhouse, J. D., Talbot, C., and Crampton, A.** In-plane vibration investigations of a noisy disc brake. In *Braking 2004: vehicle braking and chassis control*, Leeds, UK, 7–9 July 2004, pp. 103–112 (Professional Engineering Publishing, London).
- 18 Goshtasby, A.** Registration of images with geometric distortions. *IEEE Trans. Geosci. Remote Sensing*, 1988, **26**(1), 60–64.
- 19 Gonzalez, R.** *Digital image processing*, 1993, pp. 189–201 (Addison-Wesley, Reading, Massachusetts).
- 20 Steel, W. P.** *Absolute displacement measurement of noisy disc brakes using holographic interferometry*. PhD Thesis, The University of Huddersfield, July 2005.
- 21 Fieldhouse, J. D. and Beveridge, C.** A visual noise investigation of a twin caliper disc brake. In *Proceedings of the 18th Annual Brake Colloquium and Engineering Display*, San Diego, California, USA, 1–4 October 2000, SAE paper 2000-01-2771, pp. 111–122 (SAE International, Warrendale, Pennsylvania).